ARTICLES
PUBLISHED ONLINE: 2 DECEMBER 2012 | DOI: 10.1038/NCHEM.1505
nature chemistry

Real-time and *in situ* monitoring of mechanochemical milling reactions

Tomislav Friščić[1,2]*, Ivan Halasz[3,4], Patrick J. Beldon[2], Ana M. Belenguer[2], Frank Adams[4], Simon A.J. Kimber[5], Veijo Honkimäki[5] and Robert E. Dinnebier[4]

Chemical and structural transformations have long been carried out by milling. Such mechanochemical steps are now ubiquitous in a number of industries (such as the pharmaceutical, chemical and metallurgical industries), and are emerging as excellent environmentally friendly alternatives to solution-based syntheses. However, mechanochemical transformations are typically difficult to monitor in real time, which leaves a large gap in the mechanistic understanding required for their development. We now report the real-time study of mechanochemical transformations in a ball mill by means of *in situ* diffraction of high-energy synchrotron X-rays. Focusing on the mechanosynthesis of metal–organic frameworks, we have directly monitored reaction profiles, the formation of intermediates, and interconversions of framework topologies. Our results reveal that mechanochemistry is highly dynamic, with reaction rates comparable to or greater than those in solution. The technique also enabled us to probe directly how catalytic additives recently introduced in the mechanosynthesis of metal–organic frameworks, such as organic liquids or ionic species, change the reactivity pathways and kinetics.

Since antiquity[1], chemical and structural transformations by mechanical milling or grinding have been central to the processing and synthesis of materials in a number of industries[2,3]. Already well established in the fields of inorganic materials[2,4], organic and inclusion chemistry[2,5–7], mechanosynthesis is now emerging as an environmentally friendly alternative to traditional solution-based reactivity in a number of areas. These include functional metal–organic materials[8–10], nanoparticle synthesis[11], asymmetric catalysis[5,12] and screening for and large-scale manufacturing of pharmaceutical forms[13,14].

These developments have been facilitated by transferring the principles of supramolecular chemistry and catalysis to mechanochemistry, and have been aided by new mechanochemical techniques where the reactivity of the precursors mixture is improved by the addition of sub-stoichiometric amounts of liquids (liquid-assisted grinding, LAG)[16] or ionic species together with liquids (ion- and liquid-assisted grinding, ILAG)[9,17].

The microscopic understanding of mechanochemical reactions involves two principal models, both developed in the context of inorganic systems. The 'hot spot' model, which explains the reactivity of high-melting-point substances through transient microscopic areas of extremely high temperature induced by milling, was used to develop a mathematical description of reactions of inorganic substances[18]. Reactions of infinite covalent solids (such as quartz and zinc sulfide) or polymers are addressed by the magma–plasma model in which mechanical shearing leads to plastic deformation, cracking and rupture to produce reactive dislocations, atoms or radicals[19]. High-energy models are not necessarily required to explain the reactions of molecular substances, and the reactivity of molecular solids under mechanochemical milling can be described with a general three-step mechanism as put forward by Kaupp[20]. This mechanism represents a general conceptual framework that describes mechanochemical reactions through three basic processes: (i) diffusion of reactants through a mobile phase (gas[21], eutectic[22] or amorphous solid[17]) and their encounter resulting in a chemical reaction, (ii) nucleation and growth of the product phase, and (iii) product separation to expose fresh reactant surface.

Gaining a good understanding of mechanochemical reactions requires observing and describing both chemical and physical changes in the reacting sample. Continuous monitoring of milling reactions is, however, difficult, as these are conducted in a rapidly moving vessel under the violent impact of grinding media (typically steel balls). Thus, mechanistic studies normally resort to a stepwise approach in which milling is periodically interrupted and the reaction mixture characterized by X-ray diffraction or spectroscopy[15,23–26]. Although reactions that are highly exothermic or involve gases can be monitored continuously by measuring the milling vessel temperature[24] or pressure[18], characterization of solid phases in the reaction still requires stepwise analysis, which has remained of limited scope and reliability.

Modern instrumentation allows spectroscopic and diffraction measurements on a sample to be conducted in significantly less than a minute, but the practical aspects of extracting and preparing a sample for analysis can be arduous, especially for systems involving liquids. This characterization issue can limit the reliability of stepwise analysis to only the more robust intermediates[25] or non-self-sustained reactions. Moreover, stepwise analysis may also be misleading in cases where dividing the mechanical treatment into segments leads to products different from those obtained from continuous milling[24,26], and is also of limited value for air-sensitive reactions, porous materials, solvates or reactions by LAG or kneading[27], where evaporation[28] or exposure to air[29] affects analysis and reaction kinetics. In cases where the reaction continues after milling has been stopped[24,30], step-by-step analysis can no longer provide a true overview of its evolution over time. Consequently, a true assessment of the reaction course would

[1]Department of Chemistry and Centre for Green Chemistry and Catalysis, McGill University, 801 Sherbrooke Street West, H3A 8B0 Montréal, Canada, [2]Department of Chemistry, University of Cambridge, Lensfield Road, Cambridge CB2 1EW, UK, [3]Department of Chemistry, Faculty of Science, University of Zagreb, Horvatovac 102a, HR-10002 Zagreb, Croatia, [4]Max-Planck-Institute for Solid State Research, Heisenbergstrasse 1, Stuttgart, D-70569, Germany, [5]Structure of Materials Group, European Synchrotron Radiation Facility, BP 220, F-38043 Grenoble Cedex, France. *e-mail: tomislav.friscic@mcgill.ca

in many cases require *in situ* analysis without disturbing the milling process.

To circumvent these issues, we have now devised an *in situ* diffraction technique for studying ball-milling mechanosynthesis. We are particularly interested in powder X-ray diffraction (PXRD), as it provides a high level of sensitivity to structural transformations. Indeed, PXRD has been used to structurally characterize materials obtained by milling, including coordination polymers and metal–organic frameworks[26,31,32]. The *in situ* technique presented herein uses high-energy (87 keV, $\lambda = 0.1427$ Å) synchrotron radiation with excellent penetrating power and a small angular opening, as required to measure Bragg scattering. This enabled us to collect time-resolved PXRD patterns with a resolution of the order of seconds (typically in 4 s intervals) while a reaction was occurring within a closed jar, itself fabricated in-house. Comparing the diffraction patterns with those simulated for known crystal structures in the Crystal Structure Database (CSD), we were able to identify reaction intermediates and products, and thus follow the conversions of crystalline phases during the reaction (see Methods). As well as monitoring the evolution of previously known crystalline phases, the described *in situ* method should, in principle, enable the observation of new phases and their structural characterization[26,31,32]. As model reactions, we targeted the mechanosyntheses of zeolitic imidazolate frameworks (ZIFs), materials that have garnered attention in gas storage and CO_2 sequestration due to their stability to heat and moisture[33]. The mechanosynthesis of ZIFs from ZnO[9] (Fig. 1a) provides a platform to monitor inorganic, metal–organic and organic solids in the contexts of environmentally friendly synthesis and modern materials.

Reactions were performed in milling jars with 3 mm walls designed from plastic (Perspex), aluminium or steel (Supplementary Methods, Figs S1–S5), with two stainless steel balls as the grinding media, and mechanochemical conversion was followed with a time resolution of seconds. We explored reactions by neat grinding, LAG with ethanol (EtOH) or *N*,*N*-dimethylformamide (DMF) as additives, and ILAG using as additives EtOH or DMF in the presence of ammonium nitrate NH_4NO_3, ammonium methanesulfonate $NH_4CH_3SO_3$ or ammonium sulfate $(NH_4)_2SO_4$. The ligands were imidazole (**HIm**), 2-methylimidazole (**HMeIm**) or 2-ethylimidazole (**HEtIm**) (Fig. 1a,b). LAG and ILAG reactions were characterized by the parameter η (in $\mu l\ mg^{-1}$). This parameter was introduced as the ratio of added liquid volume to the mass of solid reactants, to facilitate the comparison of mechanochemical and solution-based reactions[34]. The mole percentages of liquids and salt additives are given with respect to ZnO and reactions were conducted on a 2 mmol scale based on zinc oxide.

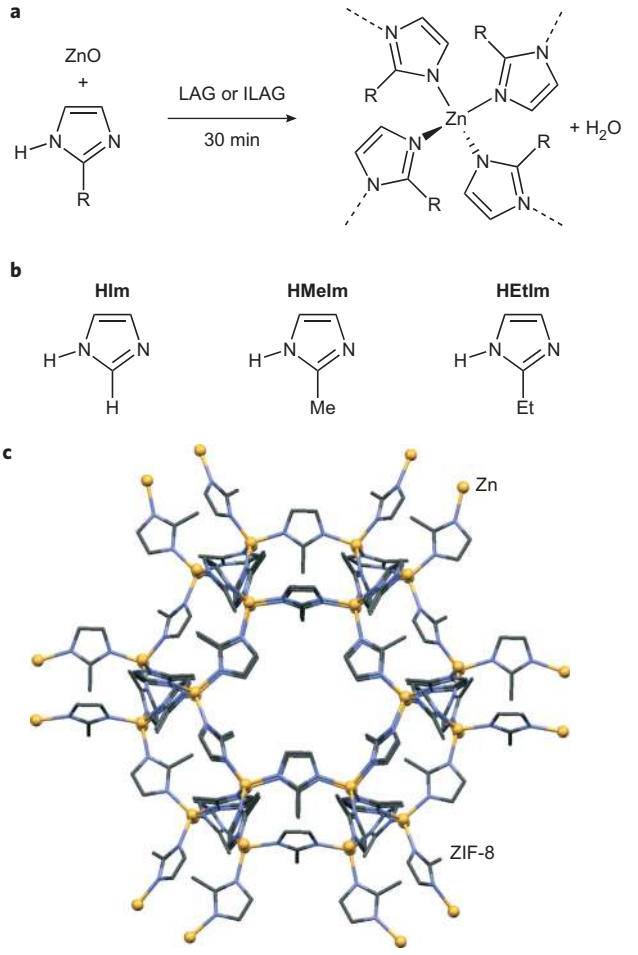

Figure 1 | The chemical reaction and participating species. a, The reactions explored in this study, conducted by milling in the presence of catalytic amounts of liquid (LAG) or catalytic amounts of liquid together with an ionic additive (ILAG). **b**, Structures of the three imidazole derivatives used as ligands. **c**, Part of the structure of one of the products, ZIF-8, which adopts the sodalite topology. The structure was drawn based on coordinates obtained from a similar crystal, previously reported[10,13] and accessible in the CSD (deposition code VELVOY).

Reactions with 2-methylimidazole (HMeIm)

The reaction of ZnO and **HMeIm** yielded the sodalite topology framework ZIF-8 (previously reported and deposited in the CSD with the code VELVOY, Fig. 1c)[33]. This framework is particularly relevant to practical applications as the only currently commercially available ZIF material (Basolite Z1200). *In situ* X-ray diffraction monitoring of the LAG (150 µl DMF, 97 mol%, $\eta = 0.31\ \mu l\ mg^{-1}$) and analogous ILAG reaction (NH_4NO_3, 5 mg, 3 mol%) demonstrated that the measured time-resolved patterns show excellent correspondence to the pattern simulated for the published crystal structure of ZIF-8[33] (Fig. 2a,b, where the intensity of reflections in the time-resolved X-ray diffractograms increases from red to blue). Plotting the time-dependent variation of the X-ray reflection with Miller indices 211 of ZIF-8 for LAG and ILAG reactions clearly demonstrated that reactivity is improved by the salt additive (Fig. 2c). In LAG, the diffraction lines of ZIF-8 became observable after ~2 min and Rietveld analysis after 30 min reveals substantial ZnO (Supplementary Figs S12–S35). In ILAG, ZIF-8 is observed almost instantaneously. Formation of ZIF-8 in time was qualitatively established by Pawley refinement[35]—a structureless approach to PXRD pattern fitting and unit cell refinement, where reflection intensities are treated as independent variables. Analysis of the PXRD pattern of the ILAG reaction (3 mol% NH_4NO_3) after 30 min milling revealed only a minor amount of residual ZnO. With 30 mg NH_4NO_3 (19 mol%; 100 µl DMF, 65 mol%, $\eta = 0.20\ \mu l\ mg^{-1}$), ZnO disappeared in 8 min (Supplementary Figs S27–S31), demonstrating a reactivity comparable to that in solution synthesis[36]. The sigmoidal LAG kinetic curve (Fig. 2c) indicates a mechanism involving nucleation and growth of product crystallites from an initially amorphous phase[37].

Reactions with 2-ethylimidazole (HEtIm)

The reaction of ZnO with **HEtIm** proceeds through the sequential formation of frameworks with the zeolite ρ (RHO, CSD code MECWOH), analcime (ANA, CSD code MECWIB)[38] and β-quartz (qtz, CSD code EHETER) topologies (Fig. 3a). *In situ* ILAG monitoring (150 µl DMF, 97 mol%, $\eta = 0.31\ \mu l\ mg^{-1}$ and 30 mg of salt, corresponding to 19 mol% NH_4NO_3, 13 mol% $NH_4CH_3SO_3$ and 12 mol% $(NH_4)_2SO_4$; Supplementary Figs S36–S49) revealed how the stepwise framework synthesis is affected by the salt. With NH_4NO_3, the

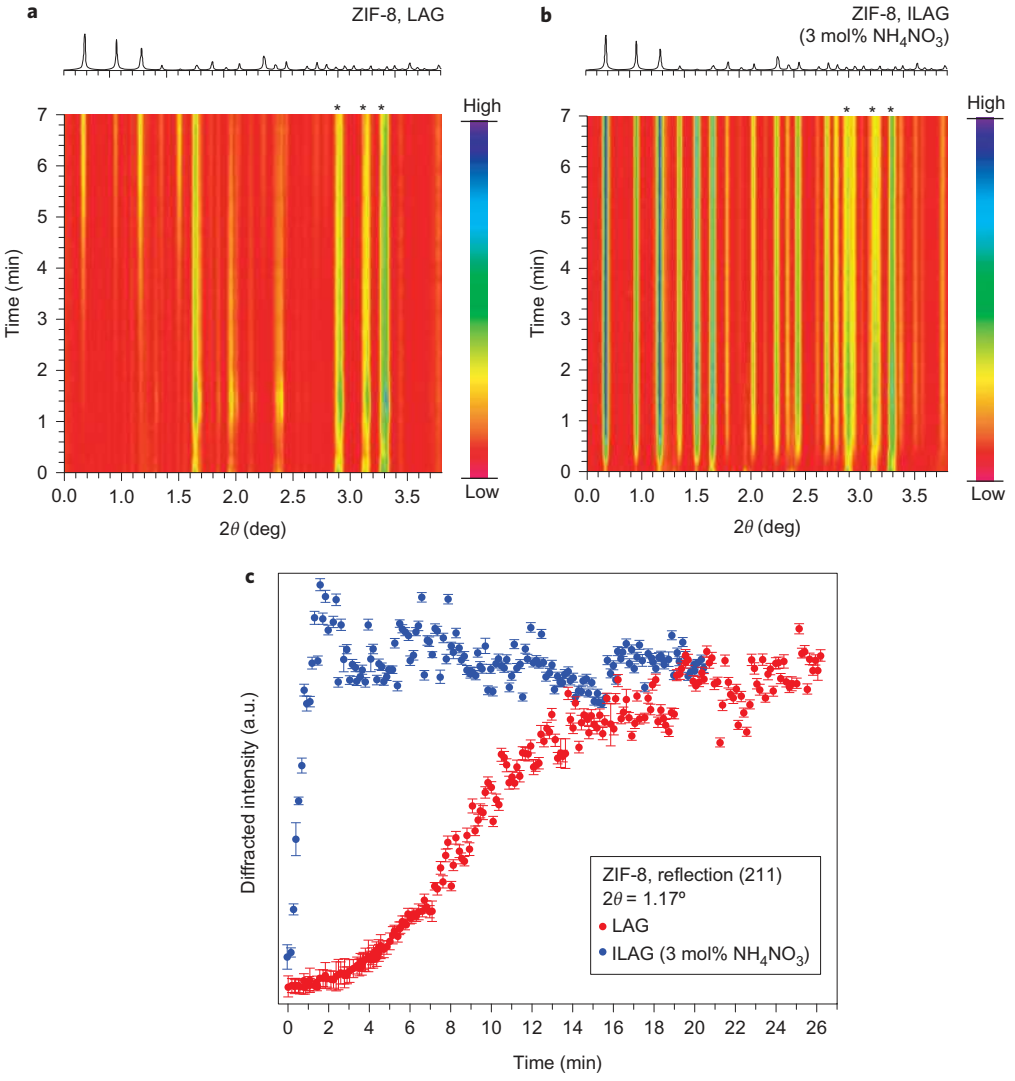

Figure 2 | Time-resolved monitoring of mechanochemical synthesis of the ZIF-8 framework from a mixture of ZnO and HMeIm ligand. a, Time-resolved diffractogram for the LAG (150 μl DMF, 97 mol%, $\eta = 0.31$ μl mg^{-1}) reaction of ZnO and **HMeIm**. **b**, Analogous ILAG reaction using 3 mol% of NH_4NO_3. **c**, Time-resolved change in the intensity of the strongest reflection (211) for the ZIF-8 product in the LAG (red) and ILAG (blue) reactions. In the time-resolved diffractograms in **a** and **b**, the reflection intensity increases from red to blue according to the colour bars provided. The simulated PXRD pattern for ZIF-8 (CSD code VELVOY) is given on top of each time-resolved diffractogram, demonstrating the correspondence of simulated and measured diffractograms. The product ZIF-8 appears almost immediately in the ILAG reaction, whereas in LAG it appears over a period of ~2 min. The positions of ZnO reflections are marked by asterisks at the top of the time-resolved diffractograms. The comparison of the development of the 211 reflection intensity of ZIF-8 with time displays a large enhancement in reaction rate and yield in ILAG when compared to the analogous LAG process. Error bars in **c** represent the standard deviation as determined from least-squares refinement of the reflection intensities according to the Pawley method.

ZnO + **HEtIm** → RHO → ANA → qtz transformation was complete in 20 min (Supplementary Movie S1). In contrast, $NH_4CH_3SO_3$ appeared to stabilize the ANA framework: the RHO → ANA transformation was accomplished in 8 min, but the ANA → qtz transformation began only after 40 min milling. ILAG with $(NH_4)_2SO_4$ was the slowest reaction, with the RHO structure being the only product for 35 min, after which point the ANA framework appeared. No reaction was observed with salt-free LAG or neat grinding (Supplementary Figs S36–S71).

Time-resolved PXRD provides previously inaccessible detail of ZIF mechanosynthesis. Time-resolved diffractograms for ILAG with different amounts of liquid (150 μl, 100 μl, 50 μl and 25 μl DMF, corresponding to 97 mol%, 65 mol%, 32 mol% and 16 mol% and $\eta = 0.28$ μl mg^{-1}, 0.18 μl mg^{-1}, 0.09 μl mg^{-1} and 0.05 μl mg^{-1}) show that product formation is delayed with decreasing η (Fig. 3, Supplementary Figs S36–S66). Plotting the time-dependent intensity of the strongest reflection for each phase enabled insight into the effect of liquid on reaction intermediates; indeed, reducing η shortened the lifetime of the ANA intermediate from ~12 min ($\eta = 0.28$ μl mg^{-1}) to 4 min ($\eta = 0.09$ μl mg^{-1}). This can be explained by the added liquid acting as a guest stabilizing the open structure of the ANA intermediate. The transformation of open ZIFs to the close-packed qtz framework requires the release of the liquid included in the framework pores, which is demonstrated by the product becoming sticky. At $\eta = 0.05$ μl mg^{-1}, ANA is not observed, suggesting either a rapid collapse into the qtz framework or a mechanism that circumvents the ANA intermediate. Other experiments support the latter: ILAG with abundant EtOH (100 μl, 86 mol%, $\eta = 0.28$ μl mg^{-1} and 30 mg NH_4NO_3, 19 mol%) also demonstrated direct conversion of RHO into the qtz framework. Although neat **HEtIm** and ZnO do not react, adding 15 mg NH_4NO_3 (14 mol%) also yielded the qtz framework with RHO as the only intermediate (Supplementary Figs S69–S71).

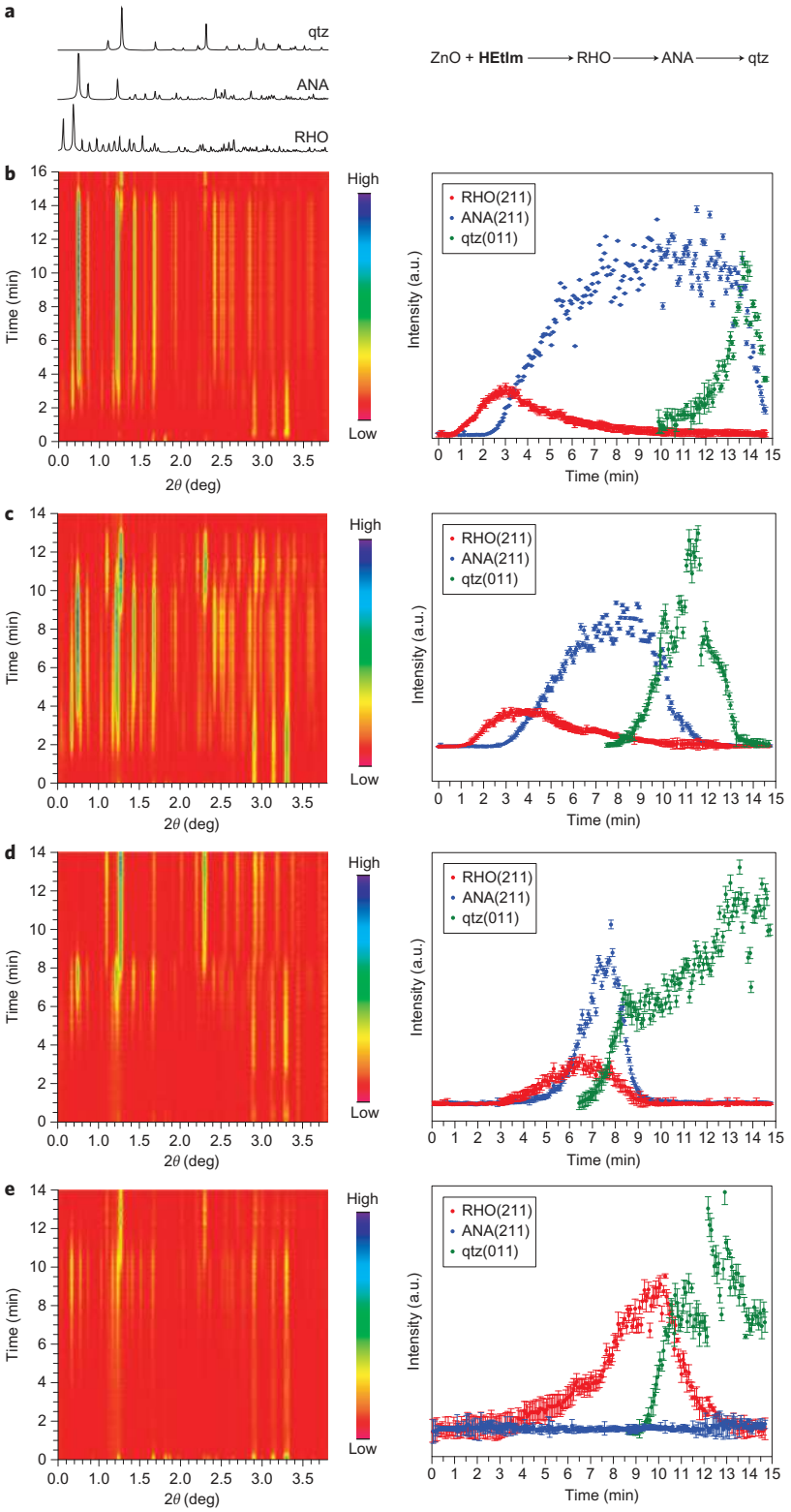

Figure 3 | Mechanochemical conversions involving the HEtIm ligand depending on the amount of added liquid. a, Simulated PXRD patterns for ZIFs based on 2-ethylimidazole (left) and the transformation of porous (RHO, ANA) to non-porous (qtz) ZIFs in the mechanochemical reaction of ZnO and **HEtIm** (right). CSD codes: qtz, EHETER; ANA, MECWIB; RHO, MECWOH. **b**–**e**, Time-resolved diffractograms (left) and variation of intensity (right) of one characteristic reflection for the RHO(211), ANA(211) and qtz(011) ZIFs in ILAG reactions involving NH_4NO_3 (30 mg, 19 mol%) and a variable amount of DMF: 150 μl (97 mol%, $\eta = 0.28$ μl mg^{-1}) (**b**); 100 μl (65 mol%, $\eta = 0.18$ μl mg^{-1}, Supplementary Movie S1) (**c**); 50 μl (32 mol%, $\eta = 0.09$ μl mg^{-1}) (**d**); 25 μl (16 mol%, $\eta = 0.05$ μl mg^{-1}) (**e**). The reflection intensities in the time-resolved diffractograms increase from red to blue according to the provided colour bars. The variation in the qtz(011) reflection intensity is an artefact of the sample adhering to the jar due to the release of the liquid previously included in the pores of intermediates. At low η (**e**), the qtz structure is obtained without the ANA intermediate, indicating a change in the reaction mechanism. Error bars represent the standard deviation determined from least-squares refinement of reflection intensities using the Pawley method.

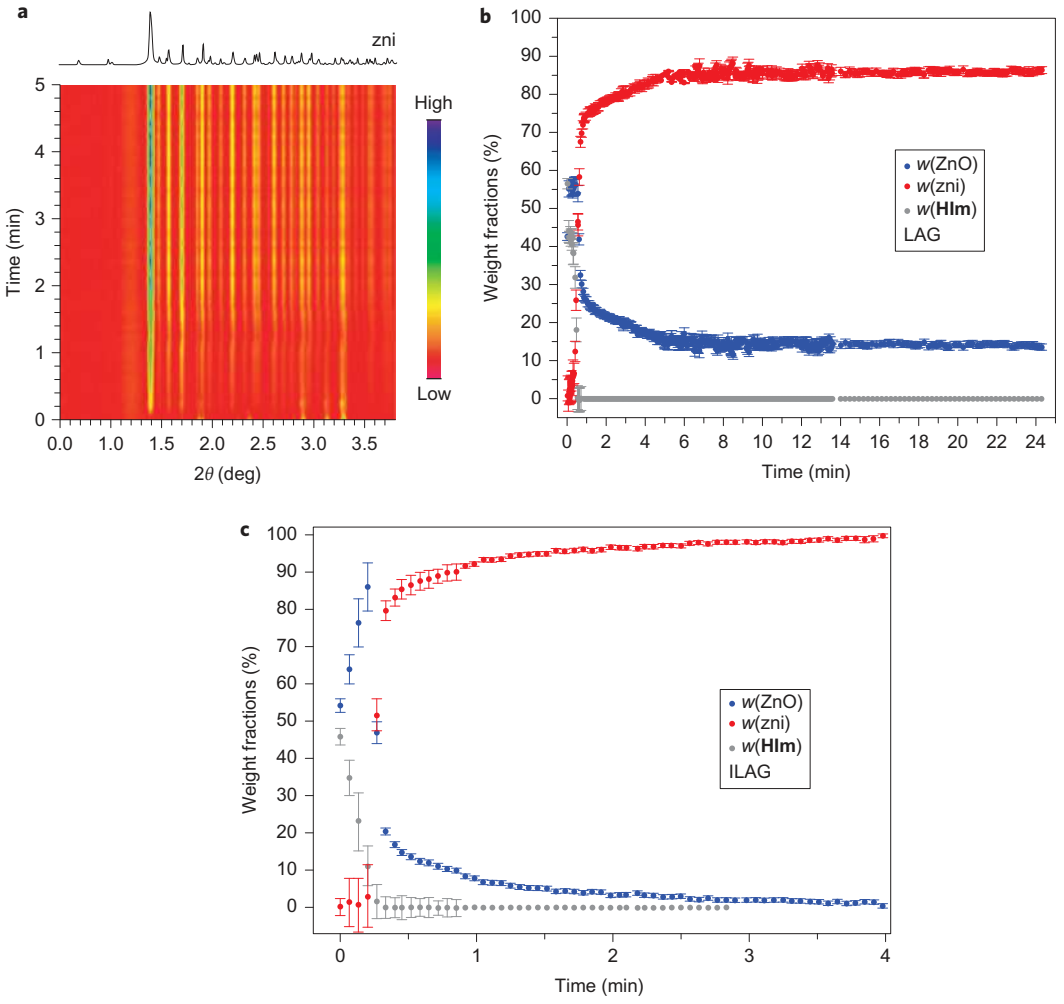

Figure 4 | Mechanochemical reactions of ZnO and HIm in the presence of ethanol. a, Time-resolved diffractogram for a selected ILAG reaction involving 150 μl EtOH (126 mol%, $\eta = 0.35\ \mu l\ mg^{-1}$) and NH_4NO_3 (15 mg, 10 mol%). The reflection intensity in the time-resolved diffractogram increases from red to blue according to the provided colour bar. The reaction in the presence of ethanol gives rise only to one type of ZIF, the non-porous zni-topology zinc(II) imidazolate (CSD code IMIDZB01), which enabled Rietveld analysis of changes in the relative fraction of crystalline reactants and products as the mechanochemical reaction proceeds. **b**, Time-dependent change in relative content of ZnO (blue), **HIm** (grey) and ZIF (red) obtained by Rietveld analysis of time-resolved X-ray diffraction data for LAG (using EtOH, top) and **c**, ILAG (using EtOH, 10 mol% NH_4NO_3, bottom) reactions. Error bars represent the standard deviation as calculated from standard deviations of variables refined in a least-squares refinement according to the Rietveld method.

Reactions with imidazole (HIm) (Rietveld analysis)

The reaction of **HIm** and ZnO takes place readily (Supplementary Figs S72–S83), with the liquid phase in LAG or ILAG directing the product topology[9,39]. *In situ* monitoring of the LAG reaction using EtOH as the grinding liquid (150 μl EtOH, 126 mol%, $\eta = 0.35\ \mu l\ mg^{-1}$) and the analogous ILAG (15 mg NH_4NO_3, 10 mol%) reaction reveals the formation of the close-packed zinc imidazolate (zni) topology framework (CSD code IMIDZB01, Fig. 4a, Supplementary Figs S78–S82)[40]. As this reaction involves only low-porosity phases, we used Rietveld analysis (Fig. 4b) to obtain relative weight fractions of crystalline substances. The refinement revealed the rapid disappearance of crystalline **HIm** (CSD code IMAZOL14), whereas the relative product fraction remained small and subsequently increased in a jump.

Rapid depletion of crystalline **HIm** probably occurs through multiple mechanisms, including amorphization, dissolution and reaction with ZnO. Crystalline ZnO is lost slowly, as shown by an artefactual increase in its weight fraction during the rapid disappearance of crystalline **HIm**, and probably mainly through chemical reaction. The effect of salt is evident both through accelerated product formation (~60 s for LAG, ~30 s for ILAG), and a higher product fraction.

Replacing EtOH with DMF (150 μl, 96 mol%) in ILAG (15 mg NH_4NO_3 10 mol%) yielded the open ZIF-4 (CSD code VEJYUF, Fig. 5a)[41] without observable intermediates (Supplementary Figs S72–S77). However, if the reaction is conducted using a smaller amount of liquid (30 μl, 19 mol%) and a larger proportion (19 mol%) of NH_4NO_3, the initially formed ZIF-4 is subsequently replaced by a structure that, according to Pawley refinement, resembles the low-porosity ZIF-6 with included water (CSD code EQOCOC) (Fig. 5b)[41]. If the reaction is conducted by neat grinding, the product is the non-porous coordination polymer $Zn_4(\mathbf{Im})_8(\mathbf{HIm})$ (CSD code KUMXEW, Supplementary Fig. S83)[42]. The formation of the non-porous structure highlights the role of the liquid in milling reactions not only for facilitating molecular diffusion[43], but also as a structure-directing agent.

Kinetic and particle size analysis

The ability to monitor mechanochemical processes *in situ* allows a detailed analysis of the underlying mechanisms, but with two caveats. First, kinetic assessment is affected by variations in the intensity of the diffracted radiation, caused by variation of the amount of diffracting material in the incident beam and by radiation

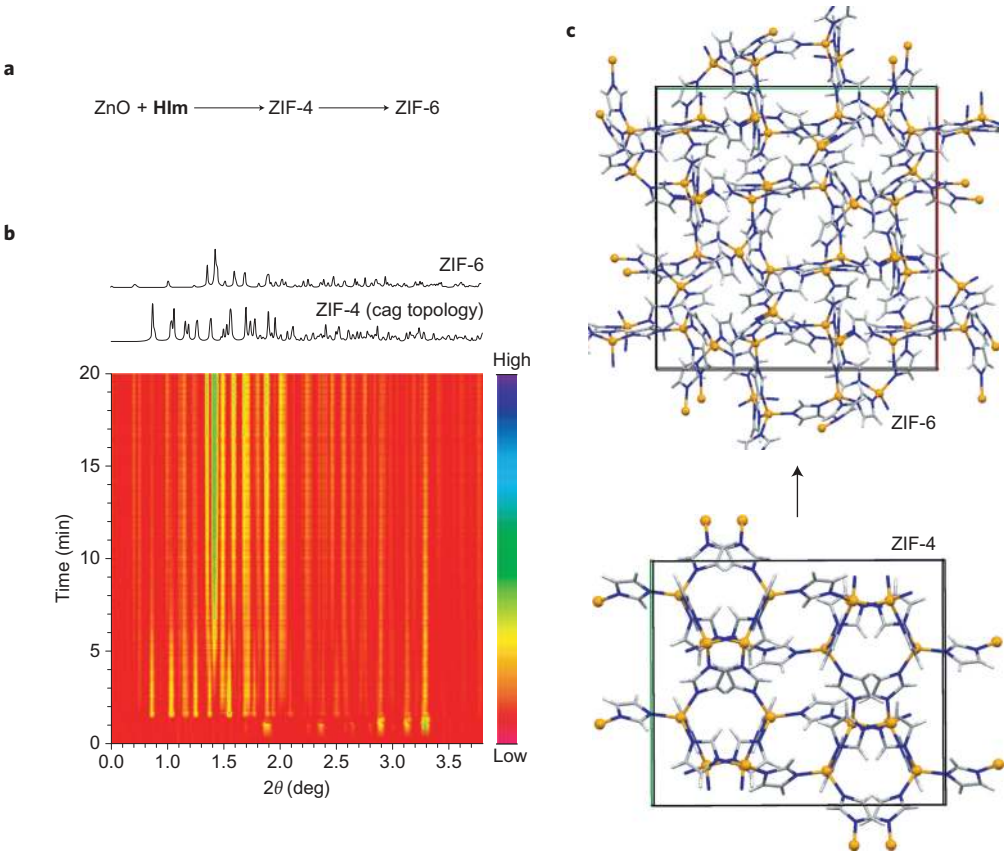

Figure 5 | Mechanochemical reactions of ZnO and HIm in the presence of DMF. a, Observed course of the stepwise mechanochemical conversion of ZnO and **HIm** into low-porosity ZIF-6 (CSD code EQOCOC), over an open-structure intermediate ZIF-4 (CSD code VEJYUF). **b**, Time-resolved diffractogram for a selected ILAG reaction involving 100 μl DMF (65 mol%, $\eta = 0.18\ \mu l\ mg^{-1}$) and NH_4NO_3 (30 mg, 19 mol%), displaying the initial appearance of ZIF-4 with characteristic X-ray reflections at approximately 0.9° and 1.1°, which subsequently disappear (within ~8 min) as the reaction gives rise to the non-porous ZIF-6 framework. **c**, Schematic of the structural transformation in the ILAG reaction described in **b**, with DMF guests in ZIF-4 omitted. The reflection intensities in the time-resolved diffractogram increase from red to blue according to the provided colour bar.

absorption by the grinding media. Without normalization to an internal standard, this prevents a rigorous analysis. Second, these reactions involve a number of substances (ZnO, ligands, products, added liquid, salt, generated water) and therefore diverge from conventional models of solid-state reactivity, such as the Avrami–Erofe'ev model (also known as Kolmogorov–Johnson–Mehl–Avrami (KJMA) or Johnson–Mehl–Avrami–Erofe'ev–Kolmogorov (JMAEK) models)[44–46] of homogeneous nucleation and growth.

With these caveats in mind, we conducted a kinetic analysis for the LAG and ILAG reactions of ZnO with **HMeIm** and with **HIm** (Figs 1, 2, 4 and 5). For reactions with **HMeIm**, we fitted the sigmoidal time dependence of the normalized ZIF-8 (211) reflection intensity (I/I_{max}, where I is the measured intensity at any point in time and I_{max} the final value of the sigmoidal part of the X-ray intensity vs. time plot) to ten solid-state reaction models[45]: the A2, A3 and A4 Avrami–Erofe'ev, the Prout–Tompkins B1, the geometrical contraction R2 and R3, and the D1, D2, D3 and D4 diffusion models (Supplementary Figs S84–S91). Initial assessment was conducted by linearizing I/I_{max} to each model.

For ILAG, the best fit was obtained with the D1 model, indicating that nucleation is kinetically not relevant in the ILAG synthesis of ZIF-8. The linearization of the data in the form of a Sharp–Hancock plot[46], as well as fitting of nonlinearized data to a general Avrami–Erofe'ev equation, were consistent with the diffusion-controlled particle growth[44,45] inherent to the D1 model. We interpret the absence of observable nucleation in ILAG as a consequence of heterogeneous nucleation from a supersaturated environment generated by rapid product formation, either on ZnO particles, milling media or the salt additive particles. For the slower LAG reaction, the data were consistent with the A2 kinetic model and diffusion-controlled product growth following deceleratory nucleation[44,46]. Fitting the data to a general Avrami–Erofe'ev model enabled us to determine the rate constants of the ILAG and LAG reactions as $k_{ILAG} = 0.0212(9)\ s^{-1}$ and $k_{LAG} = 0.00158(1)\ s^{-1}$.

Bearing in mind that the complexity of reactions demands caution in the interpretation of these results, the ability to use *in situ* data for quantitative comparisons of mechanochemical reactions is clear. The variation in diffracted intensities is particularly strong for the ZnO + **HIm** reactions, where the grinding liquid is not absorbed into the product and therefore causes the solid to temporarily adhere to the grinding jar walls. We expected that calculating the ratio of the reactant and product intensities (I_{ZnO}/I_{ZIF}) could cancel out variations and enable mechanistic insight. Indeed, the I_{ZnO}/I_{ZIF} ratios for LAG and ILAG yield largely smooth curves (Supplementary Fig. S87). If ZIF nucleation and growth occur at a similar rate to the disappearance of ZnO, the I_{ZnO}/I_{ZIF} plotted versus time should follow a $(1-x)/x$ law. This simplified view appears true for LAG. For ILAG, I_{ZnO}/I_{ZIF} drops more rapidly, indicating that ZnO dissolution is faster than ZIF growth. The above considerations indicate that ZnO reactivity is not necessarily tied to ZIF nucleation and growth.

The variation of diffracted X-ray linewidths enables particle size evolution to be monitored. Again, there is a caveat: estimating particle size requires a known instrument contribution to linewidths. The design of our experiments introduces ambiguity in that sense

(Supplementary Section S1) and, although the particle size evolution trends are reliable, absolute values should be interpreted with caution. For almost all the reactions from Figures 1 to 5, linewidth analysis indicated particle sizes ranging from 50 nm to 75 nm, with particle size equilibrium[47] established within minutes (Supplementary Figs S6–S11). The exception is the ILAG synthesis of ZIF-8, where particle size quickly peaked at ~82 nm, but was reduced at a diminishing rate to ~65 nm after 12 min. The large particle size at the beginning of the reaction is consistent with kinetic analysis that indicated rapid growth of the ZIF-8 phase under conditions of high supersaturation, thus resulting in large crystallites that fracture upon milling.

Conclusions and outlook

We have devised a method for *in situ* X-ray diffraction monitoring of mechanosyntheses in a ball mill. The benefits of this methodology are that it allows the real-time characterization and monitoring of crystalline solids without disturbing the milling process, including transformations of reaction intermediates and the indirect detection of amorphous phase (for example, by the disappearance of crystalline organic reactant). This methodology circumvents the limitations of stepwise analysis for self-sustained reactions, as the reactions studied here are known to continue after milling.

The information obtained *in situ* can subsequently be used for Rietveld analysis, fitting of kinetic models or for real-time assessment and monitoring of particle size. At present, these quantitative aspects are limited primarily by the random variations of sample amount in the incident beam, the ambiguity of instrumental linewidth contribution, and the inability to conduct rigorous Rietveld analysis on porous structures. The first difficulty is significant for samples containing a liquid, and we are confident it can be resolved by using a suitable internal standard, as indicated by the smooth curves obtained by calculating reactant/product diffraction intensity ratios. Rietveld analysis depends on the availability of crystallographic data or modelling tools that can address the amount and distribution of diverse guests in porous structures.

The recent developments[48] that enable the modelling of simple guests CH_4 or CO_2 in porous metal–organic frameworks hold the promise that modelling of more complex guests will become addressable in the near future. The diversity of phases detected in the present work clearly indicates that this *in situ* technique should be applicable to inorganic, metal–organic, organic and supramolecular (for example co-crystallization) reactions. This expectation is further supported by the wavelength tunability when using a synchrotron source, which makes the experimental conditions adaptable to materials with widely diverse X-ray scattering and absorption properties.

Methods

Experimental detail. The experiments were conducted at the European Synchrotron Research Facility (ESRF) beamline ID15B in a modified MM200 Retsch mill operating at 30 Hz. Each reaction was conducted in a jar with a volume of 10 ml using two stainless steel balls with diameters of 7 mm. In a typical experiment, 2 mmol of ZnO and the equivalent amount (4 mmol) of imidazole ligand were used as reactants, together with the additional liquid and/or salt additive. The sample temperature after a typical 20 min experiment was 33–35 °C. Incident X-rays were selected using a bent Laue silicon crystal, and the beam area at the sample was 300 μm^2. Diffracted X-rays were detected with a flat-panel Pixium charge-coupled detector. Each diffractogram was typically obtained by summing 10 frames, each collected with an exposure time of 0.4 s, giving a time resolution of 4 s between successive diffractograms. The data frames were integrated to provide plots of X-ray intensity versus the scattering angle. Reaction intermediates and products were identified by comparing the measured PXRD patterns with those simulated for known structures in the Crystal Structure Database (version 5.2, November 2010, five updates). Details of the experiments, data processing and illustrations of the experiment (Supplementary Figs S1–S5) are provided in the Supplementary Information. Milling jars were fabricated in house from transparent poly(methylmethacrylate) (Perspex, Supplementary Fig. S1), steel or aluminium. Perspex jars were used for LAG and ILAG, and metallic jars for neat grinding. All jars were constructed from two complementary parts that snapped together easily and did not leak liquid during the experiments.

PXRD. The incident energy and detector distance (1,225.76 mm) were calibrated using a NIST CeO_2 standard sample and the Fit2D software package (ESRF Internal Report, ESRF98HA01T, FIT2D V9.129 Reference Manual V3.1, 1998). Raw data frames were integrated using Fit2D. The background for each pattern was subtracted using the Sonneveld–Visser algorithm[49] implemented in Powder3D[50]. Figures were prepared using Mathematica (Version 8.0. Wolfram Research, 2010). To reduce contrast between stronger and weaker reflections, intensities were scaled by a standard procedure taking the square root or a different power of the intensity (typically 1/1.5 or 1/1.3). Pawley[35] and Rietveld[51] refinements were carried out using Topas (version 4.2. Bruker-AXS).

Pawley, Rietveld and kinetic analysis. Diffraction patterns of porous ZIFs were fitted using the structureless (Pawley) method of reflection intensity refinement. Unit cell, profile parameters, coefficients of shifted Chebyshev polynomials for background and sample particle size contribution were included in the refinements. Kinetic analysis for linearized and nonlinearized data was performed using DataFit (version 9.0.59, 1995–2008 Oakdale Engineering).

Received 5 March 2012; accepted 19 October 2012; published online 2 December 2012

References

1. Takacs, L. Quicksilver from cinnabar: the first documented mechanochemical reaction? *J. Minerals Metals Mater. Soc.* **52,** 12–13 (2000).
2. James, S. L. *et al.* Mechanochemistry: opportunities for new and cleaner synthesis. *Chem. Soc. Rev.* **41,** 413–447 (2012).
3. Baláž, P. & Dutková, E. Fine milling in applied mechanochemistry. *Miner. Eng.* **22,** 681–694 (2009).
4. Janot, R. & Guérard, D. Ball-milling in liquid media: applications to the preparation of anodic materials for lithium-ion batteries. *Prog. Mater. Sci.* **50,** 1–92 (2005).
5. Bruckmann, A., Krebs, A. & Bolm, C. Organocatalytic reactions: effects of ball milling, microwave and ultrasound irradiation. *Green Chem.* **10,** 1131–1141 (2008).
6. Stolle, A., Szuppa, T., Leonhardt, S. E. S. & Ondruschka, B. Ball milling in organic synthesis: solutions and challenges. *Chem. Soc. Rev.* **40,** 2317–2329 (2011).
7. Lazuen-Garay, A., Pichon, A. & James, S. L. Solvent-free synthesis of metal complexes. *Chem. Soc. Rev.* **36,** 846–855 (2007).
8. Adams, C. J., Haddow, M. F., Lusi, M. & Orpen, A. G. Crystal engineering of lattice metrics of perhalometallate salts and MOFs. *Proc. Natl Acad. Sci. USA* **107,** 16033–16038 (2010).
9. Beldon, P. J. *et al.* Rapid room-temperature synthesis of zeolitic imidazolate frameworks by using mechanochemistry. *Angew. Chem. Int. Ed.* **49,** 9640–9643 (2010).
10. André, V. M. *et al.* Mechanosynthesis of the metallodrug bismuth subsalicylate from Bi_2O_3 and structure of bismuth salicylate without auxiliary organic ligands. *Angew. Chem. Int. Ed.* **50,** 7858–7861 (2011).
11. Baláž, P. & Dutková, E. Mechanochemistry of sulphides, from minerals to advanced nanocrystalline materials. *J. Therm. Anal. Cal.* **90,** 85–92 (2007).
12. Rodríguez, B., Bruckmann, A., Rantanen, T. & Bolm, C. Solvent-free carbon–carbon bond formations in ball mills. *Adv. Synth. Catal.* **349,** 2213–2233 (2007).
13. Delori, A., Friščić, T. & Jones, W. The role of mechanochemistry and supramolecular design in the development of pharmaceutical materials. *CrystEngComm* **14,** 2350–2362 (2012).
14. Daurio, D., Medina, C., Saw, R., Nagapudi, K. & Alvarez-Núñez, F. Application of twin screw extrusion in the manufacture of cocrystals, part I: four case studies. *Pharmaceutics* **3,** 582–600 (2011).
15. Nguyen, K. L., Friščić, T., Day, G. M., Gladden, L. F. & Jones, W. *Nature Mater.* **6,** 206–209 (2007).
16. Friščić, T. *et al.* Ion- and liquid-assisted grinding: improved mechanochemical synthesis of metal–organic frameworks reveals salt inclusion and anion templating. *Angew. Chem. Int. Ed.* **49,** 712–715 (2010).
17. Friščić, T. & Jones, W. Recent advances in understanding the mechanism of cocrystal formation via grinding. *Cryst. Growth Des.* **9,** 1621–1637 (2009).
18. Urakaev, F. Kh. & Boldyrev, V. V. Mechanism and kinetics of mechanochemical processes in comminuting devices 1. Theory. *Powder Technol.* **107,** 93–107 (2000).
19. Gutman, E. M. *Mechanochemistry of Materials* (Cambridge International Science, 1998).
20. Kaupp, G. Solid-state molecular syntheses: complete reactions without auxiliaries based on the new solid-state mechanism. *CrystEngComm* **5,** 117–133 (2003).
21. Rastogi, R. P. & Singh, N. B. Solid-state reactivity of picric acid and substituted hydrocarbons. *J. Phys. Chem.* **72,** 4446–4449 (1968).

22. Rothenberg, G., Downie, A. P., Raston, C. L. & Scott, J. L. Understanding solid/solid organic reactions. *J. Am. Chem. Soc.* **123,** 8701–8708 (2001).
23. Tumanov, I. A., Achkasov, A. F., Boldyreva, E. V. & Boldyrev, V. V. Following the products of mechanochemical synthesis step by step. *CrystEngComm* **13,** 2213 (2011).
24. Takacs, L. Self-sustaining reactions induced by ball milling. *Prog. Mater. Sci.* **47,** 355–414 (2002).
25. Cinčić, D., Friščić, T. & Jones, W. Stepwise mechanism for the mechanochemical synthesis of halogen-bonded cocrystal architectures. *J. Am. Chem. Soc.* **130,** 7524–7525 (2008).
26. Štrukil, V. *et al.* Towards an environmentally-friendly laboratory: dimensionality and reactivity in the mechanosynthesis of metal–organic compounds. *Chem. Commun.* **46,** 9191–9193 (2010).
27. Braga, D. *et al.* Mechanochemical preparation of molecular and supramolecular organometallic materials and coordination networks. *J. Chem. Soc. Dalton Trans.* 1249–1263 (2006).
28. Braga, D., Grepioni, F. & Lampronti, G. I. Supramolecular metathesis: co-former exchange in co-crystals of pyrazine with (*R,R*)-, (*S,S*)-, (*R,S*)- and (*S,S*/*R,R*)-tartaric acid. *CrystEngComm* **13,** 3122–3124 (2011).
29. Bowmaker, G. A. *et al.* Solution and mechanochemical syntheses, and spectroscopic and structural studies in the silver(I) (bi-)carbonate: triphenylphosphine system. *J. Chem. Soc. Dalton Trans.* **40,** 7210–7218 (2011).
30. Ibrahim, A. Y., Forbes, R. T. & Blagden, N. Spontaneous crystal growth of co-crystals: the contribution of particle size reduction and convection mixing of the co-formers. *CrystEngComm* **13,** 1141–1152 (2011).
31. Fujii, K. *et al.* Direct structure elucidation by powder X-ray diffraction of a metal–organic framework material prepared by solvent-free grinding. *Chem. Commun.* **46,** 7572–7574 (2010).
32. Adams, C. J., Haddow, M. F. & Orpen, A. G. Crystal synthesis of 1,4-phenylenediamine salts and coordination networks. *CrystEngComm* **13,** 4324–4331 (2011).
33. Zhang, J-P., Zhang, Y-B., Lin, J-B. & Chen, X-M. Metal azolate frameworks: from crystal engineering to functional materials. *Chem. Rev.* **112,** 1001–1033 (2012).
34. Friščić, T., Childs, S. L., Rizvi, S. A. A. & Jones, W. Qualitative view of the role of solvent in mechanochemical and sonochemical cocrystal formation: a solubility-based approach for predicting cocrystallisation outcome. *CrystEngComm* **11,** 418–426 (2009).
35. Pawley, G. S. Unit-cell refinement from powder diffraction scans. *J. Appl. Crystallogr.* **14,** 357–361 (1981).
36. Venna, S. R., Jasinski, J. B. & Carreon, M. A. Structural evolution of zeolitic imidazolate framework–8. *J. Am. Chem. Soc.* **132,** 18030–18033 (2010).
37. Cravillon, J. *et al.* Fast nucleation and growth of ZIF-8 nanocrystals monitored by time-resolved *in situ* small-angle and wide-angle X-ray scattering. *Angew. Chem. Int. Ed.* **50,** 8067–8081 (2011).
38. Huang, X-C., Lin, Y-Y., Zhang, J-P. & Chen, X-M. Ligand-directed strategy for zeolite-type metal–organic frameworks: zinc(II) imidazolates with unusual zeolitic topologies. *Angew. Chem. Int. Ed.* **45,** 1557–1559 (2006).
39. Fernández-Bertrán, J., Castellanos-Serra, L., Yee-Madeira, H. & Reguera, E. Proton transfer in solid state: mechanochemical reactions of imidazole with metallic oxides. *J. Solid State Chem.* **147,** 561–564 (1999).
40. Spencer, E. C., Angel, R. J., Ross, N. L., Hanson, B. E. & Howard, J. A. K. Pressure-induced cooperative bond rearrangement in a zinc imidazolate framework: a high-pressure single-crystal X-ray diffraction study. *J. Am. Chem. Soc.* **131,** 4022–4026 (2009).
41. Park, K. S. *et al.* Exceptional chemical and thermal stability of zeolitic imidazolate frameworks. *Proc. Natl Acad. Sci. USA* **103,** 10186–10191 (2006).
42. Martins, G. A. V. *et al.* The use of ionic liquids in the synthesis of zinc imidazolate frameworks. *J. Chem. Soc. Dalton Trans.* **39,** 1758–1762 (2010).
43. Bowmaker, G. A., Hanna, J. V., Skelton, B. W. & White, A. H. Solvent-assisted solid-state synthesis: separating the chemical from the mechanical in mechanochemical synthesis. *Chem. Commun.* 2168–2170 (2009).
44. Cumbrera, F. L. & Sánchez-Bajo, F. The use of JMAYK kinetic equation for the analysis of solid-state reactions: critical considerations and recent interpretations. *Thermochim. Acta* **266,** 315–330 (1995).
45. Khawam, A. & Flanagan, D. R. Solid-state kinetic models: basics and mathematical fundamentals. *J. Phys. Chem. B* **110,** 17315–17328 (2006).
46. Williams, G. R. & O'Hare D. O. *J. Phys. Chem. B* **110,** 10619–10629 (2006).
47. Baláž, P. *Mechanochemistry in Nanoscience and Minerals Engineering* (Springer-Verlag, 2010).
48. Wilmer, C. E. *et al.* Large-scale screening of hypothetical metal–organic frameworks. *Nature Chem.* **4,** 83–89 (2012).
49. Sonneveld, E. J. & Visser, J. W. Automatic collection of powder data from photographs. *J. Appl. Crystallogr.* **8,** 1–7 (1975).
50. Hinrichsen, B. Dinnebier, R. E. & Jansen, M. Powder3D: an easy to use program for data reduction and graphical presentation of large numbers of powder diffraction patterns. *Z. Kristallogr.* **23** (Suppl), 231–236 (2006).
51. Rietveld, H. M. A profile refinement for nuclear and magnetic structures. *J. Appl. Crystallogr.* **2,** 65–71 (1969).

Acknowledgements

The authors acknowledge financial support from the Herchel Smith Fund, the British Council/DAAD (grant no. 1377), ESRF Grenoble, NanoDTC, the University of Cambridge and the Ministry of Science, Education and Sports of the Republic of Croatia, as well as a research fellowship (T.F.) and a doctoral fellowship (P.J.B.). McGill University and FQRNT Centre for Green Chemistry and Catalysis are acknowledged for support. The authors thank A.K. Cheetham for comments, W. Jones for support in acquiring the instrumentation and R.C. Nightingale for equipment design and manufacture. The assistance of A. Kovač and V. Dunjko with graphics preparation is acknowledged.

Author contributions

The research was organized by T.F., I.H. and R.E.D. Experiments were performed by T.F., I.H., P.J.B., A.M.B., F.A., S.A.J.K. and V.H. Data analysis was performed by I.H., S.A.J.K., T.F., P.J.B. and R.E.D. The manuscript was written by T.F. and I.H., and graphical materials were prepared by I.H., T.F. and P.J.B.

Additional information

Supplementary information and chemical compound information are available in the online version of the paper. Reprints and permission information is available online at http://www.nature.com/reprints. Correspondence and requests for materials should be addressed to T.F.

Competing financial interests

The authors declare no competing financial interests.